

Experimental and numerical investigation of fracture conductivity between non-smooth rock surfaces with and without proppant

Zihao Li^a, Ruichang Guo^b, Hongsheng Wang^b, Yuntian Teng^c, Nino Ripepi^d, Carlos A. Fernandez^a, Cheng Chen^{e,*}

^a Energy and Environment, Pacific Northwest National Laboratory, Richland, WA, 99354, USA

^b Bureau of Economic Geology, University of Texas at Austin, Austin, TX, 78758, USA

^c Hildebrand Department of Petroleum and Geosystems Engineering, University of Texas at Austin, Austin, TX, 78758, USA

^d Department of Mining and Minerals Engineering, Virginia Tech, Blacksburg, VA, 24061, USA

^e Department of Civil, Environmental and Ocean Engineering, Stevens Institute of Technology, Hoboken, NJ, 07030, USA

ARTICLE INFO

Keywords:

Proppant
Fracture conductivity
Non-smooth surface
Lattice Boltzmann
Hydraulic fracturing

ABSTRACT

The enhancement of fracture conductivity is vital for the efficient recovery of subsurface resources, such as geothermal energy and petroleum hydrocarbons. Proppants, granular materials injected into hydraulic fractures to maintain their conductivity, have been studied primarily in the context of smooth fractures (i.e., fractures between smooth rock surfaces). However, non-smooth fractures (i.e., fractures between rough rock surfaces) are common in geoenergy reservoirs and thus require further investigations. In this study, we conducted laboratory measurements of fracture conductivity on shale slabs with non-smooth surfaces and carried out numerical simulation using the lattice Boltzmann (LB) method, which aimed to investigate the conductivity of non-smooth fractures with and without proppants placement. When ceramic proppant with an areal concentration of 2 lb/ft² was placed in the fracture, the conductivity was enhanced by roughly 3 to 8 times compared to fractures without proppant. In fractures with proppant, gas-measured conductivity was higher than that measured with water due to proppant embedment caused by water. The experiments demonstrate the advantages of using proppant in fractures, even if the rock surface roughness can provide certain fracture conductivity via the self-propping mechanism. For fractures without proppants, high rock surface roughness is not necessarily favorable for enhancing fracture conductivity because the self-propping mechanism requires shear slip along the fracture surface. If there is no shear slip, high rock surface roughness can cause a detrimental effect on the fracture conductivity due to the interlocking effect. Utilizing advanced experimental equipment and LB modeling, this research explores the interplays between proppant placement, fracture geometry, and stress conditions to develop a comprehensive understanding of the productivity in non-smooth fractures. The outcomes of this investigation indicate the importance of creating fractures with surface roughness during hydraulic fracturing and will contribute to the development of more efficient stimulation techniques for subsurface energy extraction.

1. Introduction

The efficient recovery of energy resources from geothermal and oil and gas reservoirs is a paramount concern for meeting the ever-growing global energy demand. The development of hydraulic fracturing and horizontal drilling has made some subsurface reservoirs recovery economically viable (Warpinski et al., 2009; Lee et al., 2011; Rahm, 2011). One significant challenge faced by the industry is the enhancement of fluid flow in naturally fractured and hydraulically stimulated

reservoirs (Ghassemi, 2012; Breede et al., 2013; Zhang et al., 2019; Li et al., 2020; Luo et al., 2023; Qu et al., 2023a, 2023b). The interconnectivity of fracture networks and their conductivity play a crucial role in determining the effectiveness of resource extraction (Ahamed et al., 2019; Nadimi et al., 2020; Phillips et al., 2020; Li et al., 2022a). Understanding the characteristics of these fractures and employing techniques to optimize their conductivity are essential for the development of sustainable and economically viable production strategies.

One such technique to enhance fracture conductivity is to use

* Corresponding author.

E-mail address: cchen6@stevens.edu (C. Chen).

proppants, which are granular materials injected into fractures to keep them open and maintain their conductivity (Cooke Jr, 1973; Liang et al., 2016; Childers et al., 2017). Fracture conductivity, defined as the product of fracture permeability and fracture width (Fan et al., 2019; Li et al., 2022b), represents the absolute volumetric fluid flow rate contributed by a unit length of the fracture, which is directly related to the productivity of the fracture. The fracture width and permeability are influenced by the quantity of proppant used and the effective stress exerted on the proppant pack (Chen et al., 2015). During the hydraulic fracturing process, a mixture of multiple proppant particles is injected into the wellbore, with smaller proppants typically introduced first, followed by larger ones. An optimal combination of small and large proppant sizes results in the highest well productivity index in ultra-low permeability formations, such as shales (Belyadi et al., 2017). Proppant concentration, also referred to as proppant areal concentration, measures the amount of proppant placed within a fracture and is defined as the mass of proppant per unit fracture surface area, usually expressed in pounds per square foot (lb/ft^2) (Fan et al., 2019; Li et al., 2022b). While proppants have been extensively studied in the context of smooth fractures (i.e., fractures between smooth rock surfaces), limited research has been conducted on their application in non-smooth fractures (i.e., fractures between rough rock surfaces), which exhibit complex geometries and varied stress distributions. Therefore, a comprehensive understanding of the effects of proppants on non-smooth fractures' conductivity is essential for optimizing reservoir stimulation techniques in both geothermal and oil and gas reservoirs.

In the study of subsurface energy systems, modeling the behavior of proppants plays a crucial role in predicting and optimizing the efficiency of resource extraction (Fan et al., 2021). Advanced numerical models are employed to accurately capture the dynamics of proppant transport, placement, and their subsequent impacts on fracture conductivity. These models incorporate various factors such as fluid flow (Han et al., 2014; Zhang et al., 2017), proppant transport (Tong and Mohanty, 2016; Huang et al., 2022), proppant embedment (Li et al., 2015; Osipov et al., 2020), fracture geometry (Warpinski et al., 2009; Gong et al., 2020), proppant distribution (Yu et al., 2015; Wang and Elsworth, 2018), and stress conditions (Deng et al., 2011; Wang and Sharma, 2018) to simulate the interactions between proppant particles and the surrounding reservoir environment. By integrating the complex interplays between these factors, these models enable researchers and engineers to gain valuable insights into the effects of proppant type, size, concentration, and placement strategies on fracture conductivity, ultimately leading to improved reservoir stimulation techniques. Furthermore, these models also provide a platform to study the long-term stability and effectiveness of proppant packs, enabling the development of more sustainable and cost-effective approaches for subsurface energy extraction in both geothermal and oil and gas reservoirs. Among these methods, the lattice Boltzmann (LB) method is an alternative method to solving the Navier-Stokes equations at a mesoscopic scale which has advantage in dealing with complex pore geometries, such as porous media and fractures (Guo et al., 2022; Ju et al., 2017; Yi et al., 2019; Wang et al., 2024a,b). Numerous studies have proven that LB direct simulation is an effective way to evaluate flow fields and permeability (Sun et al., 2013; Vijaybabu and Dhinakaran, 2019; Wang et al., 2021). In addition, surface profile scanning technologies developed in recent years measure and analyze the topography of a surface, thereby providing detailed data of fine-scale roughness on a rock surface (Fardin et al., 2004; Tonietto et al., 2019; Salvini et al., 2020). Wang et al. (2024a,b) also developed a numerical method for quantifying fracture roughness. The combination of LB direct simulation and profilometer scans enables the accurate evaluation of the hydraulic properties in a fracture.

This study used both experimental and simulation methods to investigate the fracture conductivity between non-smooth shale slab surfaces with and without proppant applications, thereby providing insights into the role of proppant in enhancing fluid flow in complex

fracture networks. Unlike conventional studies that focus primarily on smooth fractures, this research targets non-smooth fractures, which are more commonly found in geoenergy reservoirs. Both liquids and gases were used in the experimental testing. These experiments provide tangible, real-world data on how different variables affect the physical properties of fractures under controlled conditions. In addition, the LB simulation can vary parameters systematically to predict outcomes under different stress conditions and fracture geometries. Through the development of laboratory experiments and implementation of advanced numerical models, this research will investigate the interactions between proppant particles, fracture geometries, and stress conditions, ultimately leading to better understanding of proppant behaviors and the potential to improve resource recovery in geothermal and oil and gas reservoirs. The outcomes of this investigation will contribute to the development of more efficient and realistic reservoir stimulation techniques, leading to increased energy productivity, reduced environmental impacts, and lower costs for both the geothermal and oil and gas industries. The findings will also provide a foundation for future research on proppant materials, fracture network optimization, and the adaptation of the latest numerical simulation techniques to reservoir engineering applications.

2. Materials and methodology

2.1. Fracture conductivity measurement

Fig. 1 illustrates the fracture conductivity measurement cell used in the experiments. This apparatus allows for the determination of proppant fracture conductivity under a range of effective stresses and temperatures. In the fracture conductivity test, the fracture conductivity is computed as the product of the fracture's permeability with the fracture width. The fracture width is gauged by the change in the chamber's height, captured by a displacement transducer. As per the American Petroleum Institute (API) RP-19D standard (2021), the fracture conductivity, C , is defined as:

$$C = kw_f = \frac{\mu \cdot Q \cdot L \cdot w_f}{\Delta p \cdot A} = \frac{\mu \cdot Q \cdot L}{\Delta p \cdot h} \quad (1)$$

where C is fracture conductivity (m^3); k is fracture permeability (m^2); w_f is fracture width (m); h is the size of the longer dimension of the fracture cross section (m); A is the area of fracture cross section and equal to $w_f h$ (m^2); μ is fluid viscosity ($\text{Pa}\cdot\text{s}$); Q is volumetric flow rate (m^3/s); L is the length over which the pressure difference is measured (m); Δp is the pressure difference (Pa). Note that μ , L , and h in Equation (1) are known. The measured flow rate and pressure difference are then imported into Equation (1) to calculate the fracture conductivity.

Fig. 2 demonstrates the non-smooth shale slabs extracted from the

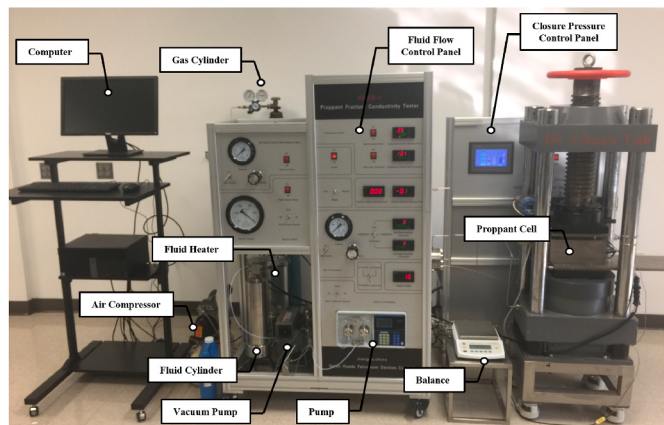


Fig. 1. Fracture conductivity measurement cell used in the study.

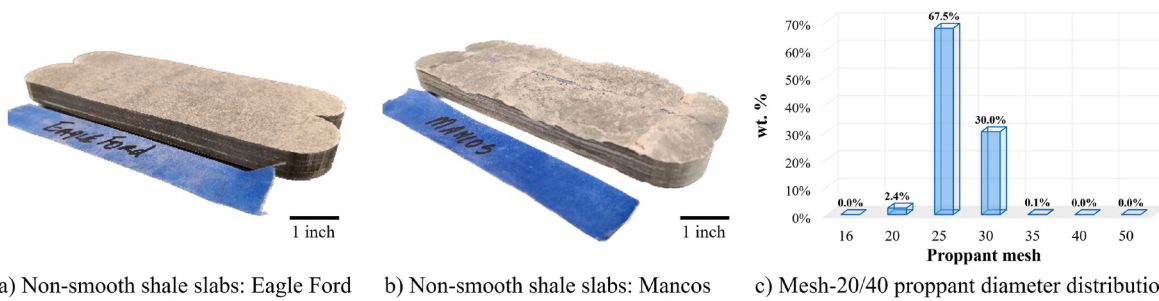


Fig. 2. Shale slabs with non-smooth surfaces extracted from a) Eagle Ford, and b) Mancos formations, and c) distribution of particle diameter for the mesh-20/40 proppant.

Eagle Ford Shale and Mancos Shale. The mineralogy and total organic carbon (TOC) of these shale slabs are given in Table 1. In particular, the rock slabs were cut surrounding a natural fracture or stratum, which was subsequently utilized as the connecting surface between the two non-smooth slabs. Each shale slab had dimensions of 7" × 1.5" × 0.5" (length × width × thickness). The effective stress was defined as the difference between the closure pressure and pore pressure. The experiments applied effective stresses of 500 psi, 1,000 psi, 1,500 psi, and 2,000 psi on the shale slabs. For the comparison between liquid and gas tests, it is essential to use the same slab pair because the non-smooth surfaces on each slab pair have a unique pattern and surface roughness. Therefore, the maximum effective stress was set at 2,000 psi to prevent damage to the rock slabs caused by excessive loading.

The proppant used in this study is CARBOECONOPROP® Low-density ceramic proppant, which is provided by CARBO Ceramics Inc, and can withstand external stresses up to 10,000 psi. The mesh size of this proppant is 20/40 with a particle diameter distribution in the range between 400 μm and 841 μm. The selection of the 20/40 proppant is based on its capacity of providing high permeability and conductivity, considerable strength and resistance to crushing, effective transport and placement in fractures, and overall cost effectiveness. These properties make the 20/40 proppant a widely used product for enhancing the productivity of hydraulically fractured wells. Fig. 2c illustrates the size distribution of the mesh-20/40 proppant.

The conductivity measurement in this paper includes measurements with proppant and without proppant placement at a temperature of 298 K using gaseous nitrogen and deionized (DI) water as the testing fluids. In those reservoirs with sensitive mineral compositions or where there is a high risk of scaling or clay swelling, DI water can avoid the introduction of additional salts and chemicals and minimize the possibility of adverse reactions. In addition, DI water can also provide a consistent and predictable base fluid for precise chemical control. As a dry gas, nitrogen can avoid clay swelling and hence prevent permeability reduction. Furthermore, nitrogen is inert and thus does not react with the formation minerals or fluids, thereby reducing the risk of formation damage from chemical reactions.

After completing material preparation, the procedure for experimentally measuring fracture conductivity is described as follows. First, the proppant with a concentration of 2 lb/ft² (Simo et al., 2013; Schmidt

et al., 2014) is sandwiched between two shale slabs. The proppant assembly is then placed inside the cell chamber. To drain air from the proppant pack when using DI water, the pore space in the proppant pack is filled with DI water to ensure saturation, while this step can be skipped when using nitrogen. Subsequently, the flow pump is switched on to achieve the target flow rate of DI water or nitrogen in the fracture, followed by turning on the back-pressure regulator and adjusting the back pressure to the desired test conditions. After that, the hydraulic pump for the effective stress is activated, and the pre-set effective stress will be applied to the chamber. Following a short duration, during which the effective stress and the flow rate of DI water or nitrogen reach a steady state, the computer starts to record the fracture conductivity value under each effective stress. It is worth noting that the correction of the Klinkenberg effect is essential after the measurement using nitrogen, and the method for the correction will be discussed in the following section.

The measurement without proppant placement in the fracture space will follow similar steps. Based on previous studies (Geng et al., 2014; Bijay and Ghazanfari, 2021), the surface roughness on rock samples enabled the fracture to self-prop without proppant placement, which can achieve considerable fracture permeability. The aim of the experiments without proppant is to study the role of rock surface's roughness on the fracture conductivity through the "self-proping" mechanism under various effective stresses. Both nitrogen and DI water were used in the experiments to study the influence of the testing fluid. To avoid embedment damage to rock surface and enable the comparison between tests, nitrogen-based measurements under effective stresses of 500, 1,000, 1,500, and 2,000 psi were first conducted without the placement of proppant in the fracture. We then conducted the DI-water-based measurements under the same effective stresses. After the completion of the experiments without proppant, the chamber was opened and ceramic proppant particles, at a concentration of 2 lb/ft², were carefully placed into the fracture space between the two slabs. In the next step, both nitrogen-based and DI-water-based measurements were repeated following the same procedures.

2.2. Correction of the Klinkenberg effect for gas-measured conductivity

During the nitrogen gas conductivity measurements, an increase in the apparent (i.e., measured) fracture conductivity was observed, which was attributed to the Klinkenberg effect that enhances apparent permeability by causing fluid slip at the solid surface (Klinkenberg, 1941; Tan et al., 2018; Li et al., 2022b). An approach of data correction is required to effectively eliminate the impact of the Klinkenberg effect and hence to obtain the absolute (i.e., true) permeability of the fracture. The relation between the apparent and absolute permeabilities is written as (Li et al., 2022a):

$$k_a = k(1 + b/p) \quad (2)$$

where k_a is the apparent permeability (m^2), k is the absolute permeability (m^2), p is the gas pressure (Pa), and b is the Klinkenberg

Table 1
Mineralogy and TOC of the Eagle Ford and Mancos shale slabs.

		Eagle Ford (wt%)	Mancos (wt%)
Mineralogy	Calcite	70	5.1
	Quartz	18	56.4
	Dolomite	2	10.9
	Albite	/	6.4
	Kaolinite	9	2.5
	Microcline	/	7.9
	Pyrite	1	1.1
	Muscovite	/	9.7
TOC		2.8	1.37

coefficient (Pa). If we plot k_a as a function of $1/p$, a linear extrapolation of the data gives the value of k , which is the intercept on the y axis; in other words, the absolute permeability is the apparent permeability measured under an infinitely large gas pressure. Fig. 3 presents two plots as an example of the Klinkenberg effect correction, which was conducted in fractures from the Eagle Ford and Mancos formations. Under each effective stress, we conducted three gas flow experiments with different gas pressures. The extrapolation method was then used to eliminate the Klinkenberg effect to obtain the absolute conductivity under this particular effective stress. The results are illustrated in Table 2. We adopted this Klinkenberg correction method for all gas-measured experiments, and thus all the gas-measured conductivity values reported in this study are the absolute conductivity values.

2.3. LB simulation

Because of the advantage in dealing with complex pore boundaries, the LB simulation was used to investigate the conductivity of fractures. A three-dimensional, 19-velocity-vector (D3Q19) model was employed in the LB simulation. A single-relaxation-time Bhatnagar–Gross–Krook approximation was employed to solve the evolution of fluid particles. The evolution equation is written as (Chen et al., 2009):

$$f_i(\mathbf{x} + \mathbf{e}_i \delta t, t + \delta t) = f(\mathbf{x}, t) - \frac{f_i(\mathbf{x}, t) - f_i^{eq}}{\tau}, (i=0, 1, 2 \dots 18) \quad (3)$$

where $f_i(\mathbf{x}, t)$ is the particle distribution function specifying the probability that fluid particles at lattice location \mathbf{x} and time t travel along the i th direction, \mathbf{e}_i is the lattice velocity vector in the D3Q19 model, and τ is the dimensionless relaxation time and related to the kinematic viscosity by $\nu = (2\tau - 1)\Delta x^2/6\Delta t$, where Δx is the lattice spacing and Δt is the time step. f_i^{eq} is the equilibrium distribution function calculated as:

$$f_i^{eq} = \rho w_i \left[1 + \frac{3\mathbf{e}_i \cdot \mathbf{u}}{c^2} + \frac{9(\mathbf{e}_i \cdot \mathbf{u})^2}{2c^4} - \frac{3\mathbf{u}^2}{2c^2} \right], (i=0, 1, 2 \dots 18) \quad (4)$$

where $c = \Delta x/\Delta t$, and the weight coefficient w_i is defined as:

$$w_i = \begin{cases} 1/3 & i = 0 \\ 1/18 & i = 1 \sim 6 \\ 1/36 & i = 7 \sim 18 \end{cases} \quad (5)$$

The macroscopic fluid density and velocity in the LB system are calculated as:

$$\rho = \sum_{i=0}^{18} f_i \quad (6)$$

$$\mathbf{u} = \sum_{i=0}^{18} f_i \mathbf{e}_i / \rho \quad (7)$$

The fluid pressure is calculated using $p = c_s^2 \rho$, where c_s is the speed of

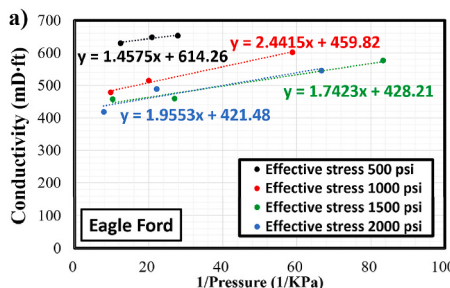


Table 2

Nitrogen-measured conductivity values of the fractures in the Eagle Ford and Mancos formations under different effective stresses. The conductivity values have been corrected to eliminate the Klinkenberg effect using the extrapolation method.

Effective stress (psi)	True conductivity (mD·ft), Eagle Ford	True conductivity (mD·ft), Mancos
500	614.3	213.6
1000	459.8	210.2
1500	428.2	208.9
2000	421.5	206.8

sound. In the D3Q19 LB model, $c_s^2 = c^2/3$. In the LB simulation, a body force was applied to drive fluid flow. The periodic boundary condition was implemented, and buffer layers were included at the two ends of the fracture to ensure smooth transition of fluid flow between the inlet and outlet of the fracture space. More details regarding the LB model can be found in our previous studies (Chen et al., 2009, 2015).

3. Results and discussion

3.1. Fracture conductivity and profilometer measurements

Fig. 4 illustrates the fracture conductivity measured under various effective stresses. These measurements were conducted in the non-smooth fractures with and without proppant placement between the rock slabs, and both nitrogen and DI water were used as the testing fluids. Based on the measurements, when the mesh-20/40 ceramic proppant with a concentration of 2 lb/ft² was placed in the fracture space, the fracture conductivity values were about three to eight times higher than those without proppant placement. This suggests that while the rock surface's roughness does offer some fracture conductivity through the “self-propping” mechanism, it is more beneficial to have proppant placement in the fractures.

For fractures filled with proppant, the conductivity values measured using nitrogen were higher than those measured using DI water. This was attributed to the softening of the rock surfaces when they were exposed to DI water, which led to proppant embedment into rock surfaces and consequently decline of the fracture conductivity. Table 1 illustrates that both the Eagle Ford and Mancos cores contained clay and carbonate minerals, which could soften the rock surface when in contact with water. In addition, when no proppant was placed in the fracture space, the conductivity values measured by nitrogen and DI water were almost the same, and the decrease in fracture conductivity with increasing effective stress was not noticeable. This suggested that when a fracture is propped only by the surface roughness (i.e., self-propping), the fracture conductivity is insensitive to the testing fluid and the effective stress.

Fig. 5 illustrates that the profilometer measurements of the rock surface topography for the non-smooth shale slabs, which were used in

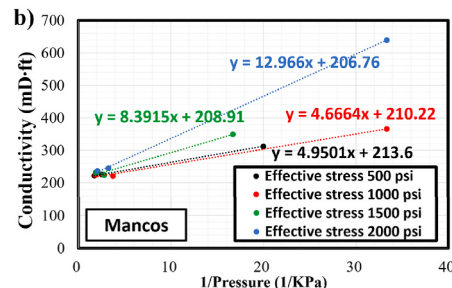


Fig. 3. Apparent conductivity of the fractures in rock slabs extracted from a) Eagle Ford, and b) Mancos formations under three different gas pressures. These gas measurements were conducted using nitrogen in empty fractures without proppant placement. Extrapolation based on the measurements under the three gas pressures eliminates the Klinkenberg effect and gives the absolute permeability and hence the true conductivity of the fracture.

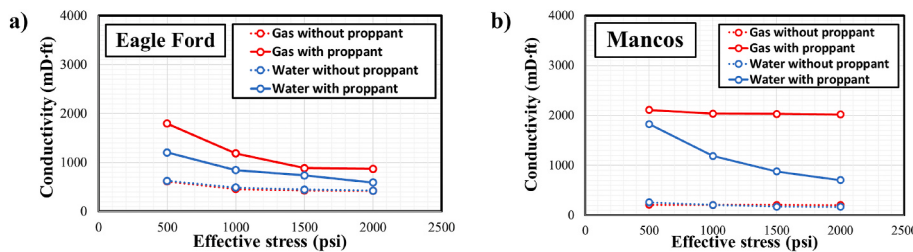
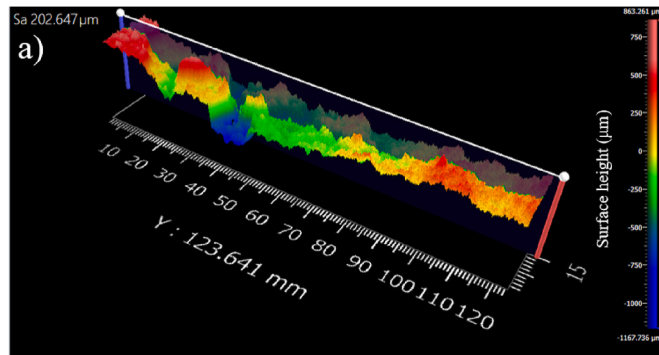
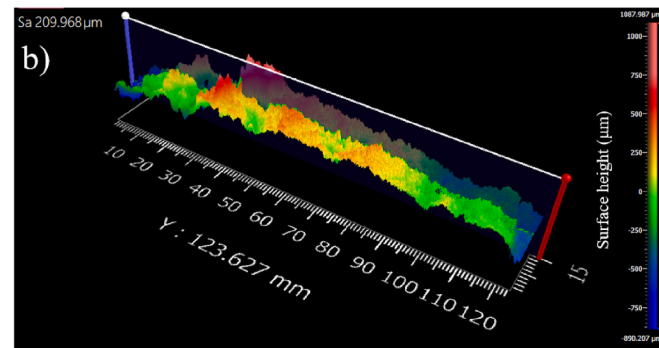


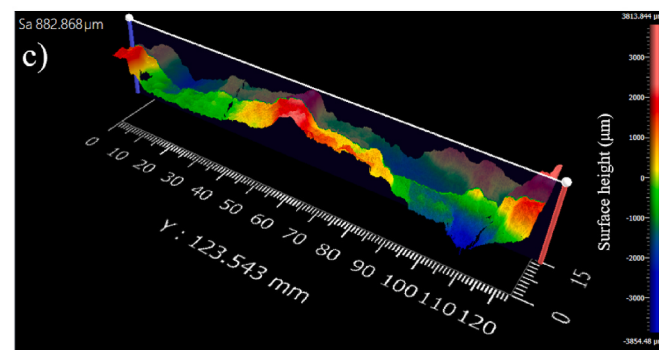
Fig. 4. Measured fracture conductivity as a function of effective stress for shale slabs extracted from a) Eagle Ford, and b) Mancos formations. “Gas” and “water” indicate that the measurements were conducted with nitrogen gas and DI water as testing fluids, respectively. The conductivity values measured with nitrogen have been corrected to eliminate the Klinkenberg effect.



a) Eagle Ford shale non-smooth slab #1



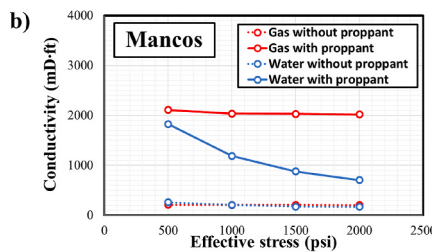
b) Eagle Ford shale non-smooth slab #2



c) Mancos shale non-smooth slab #1

Fig. 5. Profilometer measurements of the non-smooth shale slabs extracted from the Eagle Ford and Mancos formations.

the fracture conductivity measurements shown in Fig. 4. Each shale slab was scanned by the profilometer and stitched using a 264-site stitch with a 5 × Super Long Working Distance (SLWD) objective. The full surface of



each slab is stitched together into a single height map with over 265 million data points. The objective of these profilometer measurements is to investigate proppant embedment on the non-smooth slab surface. The high effective stress during the test led to the damage of one shale slab (Mancos slab #2), thereby disqualifying it for profilometer scans. The remaining samples (Mancos slab #1 and Eagle Ford slabs #1 and #2) were scanned with full-sample stitches.

The arithmetical mean height, S_a , measures the height difference of each point from the average height of a surface. This value is typically used to gauge surface roughness. As illustrated in Fig. 5, the S_a values of Eagle Ford slab #1, Eagle Ford slab #2, and Mancos slab #1 were 202.647 μm, 209.968 μm, and 882.868 μm, respectively. These measurements quantitatively indicate that the Eagle Ford slabs were considerably smoother than the Mancos slab, which is consistent with visual observations of the laboratory pictures (Fig. 2).

3.2. Non-smooth fractures versus smooth fractures

To compare the productivity between non-smooth fractures and smooth fractures, Fig. 6 illustrates the DI water-measured fracture conductivity values of Eagle Ford, Mancos, and Marcellus slabs. Particularly, the data for the Eagle Ford and Mancos slabs are from Fig. 4 (i.e., non-smooth fractures), whereas the data for the Marcellus slabs were measured in a smooth fracture (Li et al., 2022b). When no proppants were placed in the fracture, the Marcellus fracture (i.e., smooth fracture) had the lowest fracture conductivity, which was expected because the two smooth fracture walls were in full contact with each other under compressive stress. The Mancos fracture, which had high surface roughness, demonstrated a lower fracture conductivity than the Eagle Ford fracture, which had moderate surface roughness. This was because the two rough rock surfaces were tightly aligned with each

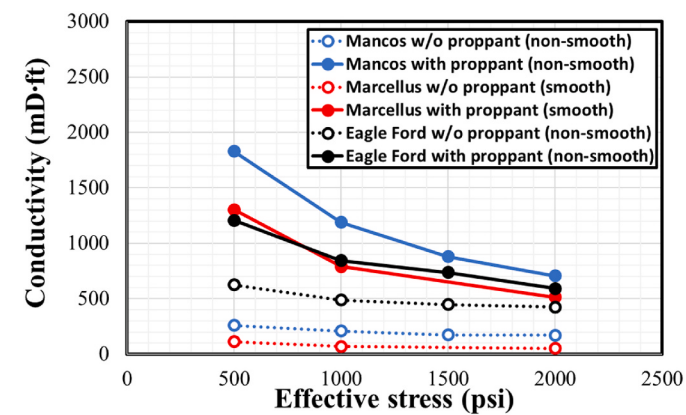


Fig. 6. DI water-measured fracture conductivity as a function of effective stress. The data for Marcellus shale slabs, which had smooth rock surfaces, are from Li et al. (2022b). The proppant concentration was 2 lb/ft² for the tests with proppant placement.

other under compressive stress without proppant placement, which is referred to as the interlocking mechanism. In this case, higher surface roughness increased the tortuosity of the flow paths within the fracture, leading to lower fracture conductivity. This suggests that high surface roughness is not necessarily favorable for enhancing fracture conductivity because the self-propping mechanism requires shear slip along the fracture surface. If there is no shear slip along the fracture surface, which is the case in the measurements without proppant placement, high surface roughness will cause a detrimental effect on the fracture conductivity due to the interlocking effect.

When proppant particles were placed in the fracture, the Mancos fracture, which had the highest surface roughness, showed the highest fracture conductivity. This was because proppant distribution was non-uniform on rough rock surfaces, which led to local particle packing that had high porosity and consequently high permeability. With the increase of rock surface roughness, the enhancement of local porosity can be promoted, which contributes to the enhancement of the overall fracture conductivity. In contrast, the fracture conductivity curves for the Eagle Ford slabs (moderate surface roughness) and Marcellus slabs (smooth surface) were similar. This was because the proppant distribution was relatively uniform between smooth and low-roughness rock surfaces, which prevented the formation of local particle packing that had high porosity. In addition, with uniform proppant packing at the proppant concentration of 2 lb/ft², the proppant assembly had approximately ten layers of particles, which was a tightly packed porous medium. In this case, the permeability of the proppant-filled fracture depended primarily on the permeability of the particle assembly and was insensitive to the rock surfaces (Fan et al., 2019). Therefore, the fracture conductivity was similar in the proppant-filled Eagle Ford and Marcellus fractures.

3.3. Conductivity-fracture width relationship based on LB simulation

The experimental findings suggested that there may be a correlation between the conductivity of a proppant-free fracture and the fracture width. This correlation is significantly influenced by the roughness of the rock surfaces, which in turn is determined by the properties of the rock minerals. We hypothesize that fractures in identical rock types share similar surface roughness characteristics. Therefore, we artificially generated rough fractures with different widths. The surface roughness was generated based on the rock surface roughness characterized in the profilometer measurements. The LB simulation was then conducted to determine the fracture permeability and consequently the fracture conductivity in these artificially-generated non-smooth fractures. Based on the profilometer measurement data, the spatial correlation of rock surface roughness on the same rock type can be determined. Particularly, the covariance of rock surface roughness as a function of the separation distance can be written as:

$$\text{Cov}(L) = \frac{1}{N} \sum_{i=1}^N \sigma(x_i) \bullet \sigma(x_i + L) - \frac{1}{N} \sum_{i=1}^N \sigma(x_i) \bullet \frac{1}{N} \sum_{i=1}^N \sigma(x_i + L) \quad (8)$$

where σ is the local rock surface roughness, x_i is the location of sample i on the rock surface, L is the separation distance, and N is the total sample number. This equation characterizes the covariance (i.e., similarity) between the roughness at two locations, separated by a distance of L , on the rock surface (Guo et al., 2020). We applied this equation to the profilometer measurement data and obtained the roughness covariance functions for the Eagle Ford and Mancos fracture surfaces, as illustrated in Fig. 7. The scatter data are from data analysis of the profilometer measurements using Equation (8), whereas the solid curve is based on data fitting using the exponential function. The spatial correlation length of a rough rock surface is defined as the separation distance at which the covariance of surface roughness is reduced to e^{-1} . Based on the data analysis, the surface roughness of the Eagle Ford fracture had a standard deviation of 10.7 μm and a spatial correlation length of 74.2 μm. The surface roughness of the Mancos fracture had a standard deviation of 19.7 μm and a spatial correlation length of 142.4 μm. Using these properties of the surface roughness, we reconstructed Eagle Ford and Mancos fractures with different fracture widths. One set of the reconstruction samples are demonstrated in Fig. 8.

LB direct simulations were then performed on the reconstructed fractures. The fracture space was resolved at a resolution of 5 μm per pixel length in the LB model. The width of the reconstructed fractures was selected in the range around the width measured in the experiments. In the simulation on the Eagle Ford fractures, the fracture width took values of 115 μm, 125 μm, 135 μm, 145 μm, 155 μm, and 165 μm. In the simulations on the Mancos fractures, the fracture width took values of 80 μm, 90 μm, 100 μm, 110 μm, and 120 μm. The fracture permeability was calculated using the LB-simulated flow field in the fracture space based on Darcy's law. The fracture conductivity was then calculated as the product of fracture permeability and fracture width based on Equation (1). Fig. 9 illustrates experimentally-measured and LB-simulated fracture conductivity against fracture width.

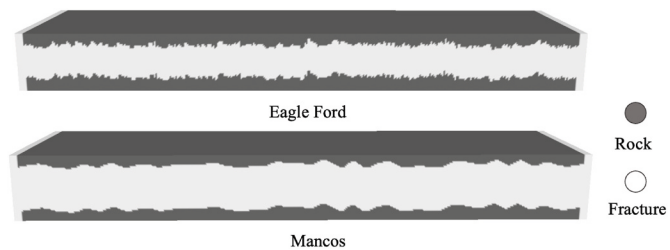


Fig. 8. Eagle Ford and Mancos fractures reconstructed using the profilometer measurement data.

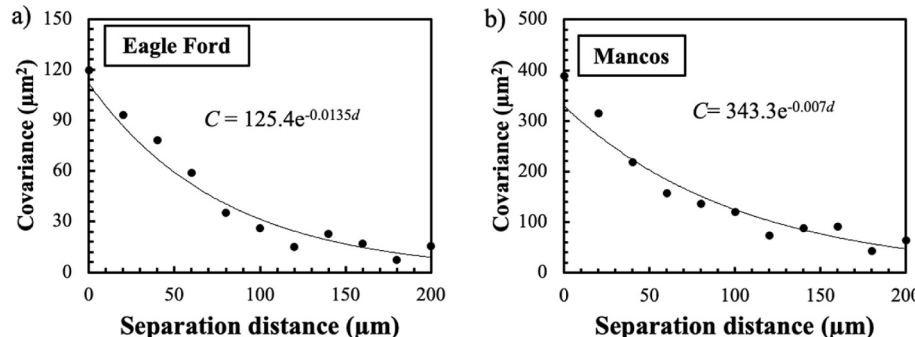


Fig. 7. Covariance of rock surface roughness as a function of separation distance in the Eagle Ford and Mancos fractures. Scatter data are from data analysis of the profilometer measurements, whereas the solid curve is data fitting using the exponential function.

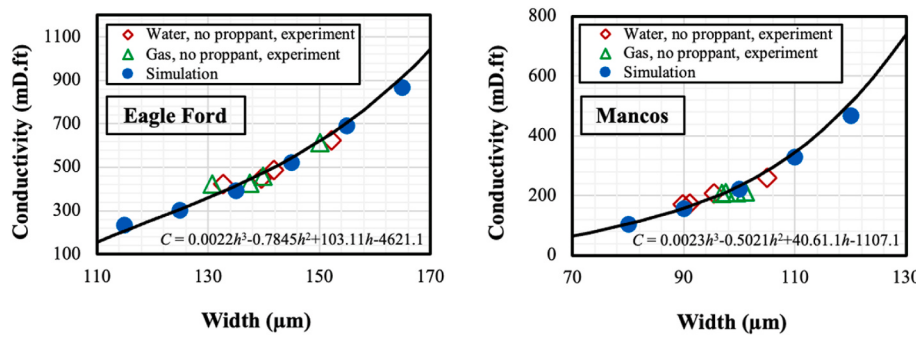


Fig. 9. Fracture conductivities for a) Eagle Ford, and b) Mancos fractures without proppant placement. The hollow data points are experimental measurements using DI water and nitrogen gas as the testing fluids, whereas the solid data points are from LB simulation. The solid curves are based on data fitting using the polynomial function.

Given the high cost of fracture conductivity measurements in the laboratory, it is beneficial to identify an empirical correlation between fracture conductivity and fracture width. The dimension analysis suggests that the relation between fracture conductivity and fracture width can be written as $C \propto h^3$. Therefore, we used a third-order polynomial function to fit the experimental and simulation data, leading to $C = 0.0022h^3 - 0.7845h^2 + 103.11h - 4621.1$ and $C = 0.0023h^3 - 0.5021h^2 + 40.61.h - 1107.1$ for the Eagle Ford and Mancos fractures, respectively. Since a fracture's hydraulic conductivity depends solely on the fracture geometry, these empirical correlations provide a cost-effective means to estimate the conductivity of empty fractures (i.e., no proppant placement) in rocks with similar surface roughness. For rocks with different roughness characteristics, the same workflow can also be employed, and only several experiments are needed to validate the simulations.

4. Conclusions

In this study, we investigated fracture conductivity between non-smooth rock surfaces with and without proppant placement. Using laboratory experiments and LB simulation, we obtained insights into the nuances of fracture behaviors when the fracture space is between non-smooth rock surfaces. The research findings underline the role that proppants play in enhancing fracture conductivity and subsurface energy recovery. The laboratory experiments showed a noticeable increase in fracture conductivity when proppants were placed, thereby confirming the importance in practical applications, even if the roughness of the rock surface can provide certain fracture conductivity by means of the self-propping effect. For fractures without proppant placement, high rock surface roughness is not necessarily favorable for enhancing fracture conductivity because the self-propping mechanism requires shear slip along the fracture surface. If there is no shear slip along the fracture surface, high rock surface roughness can cause a detrimental effect on the fracture conductivity due to the interlocking effect. Furthermore, the LB simulation provided advanced understanding of the fracture dynamics at the microscopic scale, leading to an empirical correlation between the conductivity of proppant-free fractures and the fracture width.

This research emphasizes the crucial role of combining laboratory experiments with numerical simulation in understanding and optimizing fracture conductivity. The insights obtained from this work indicate the benefit of creating non-smooth fractures during hydraulic fracturing, which provides a more productive way for subsurface energy development.

CRediT authorship contribution statement

Zihao Li: Writing – review & editing, Writing – original draft, Visualization, Validation, Software, Methodology, Investigation, Formal

analysis, Data curation, Conceptualization. **Ruichang Guo:** Writing – review & editing, Writing – original draft, Software, Methodology, Investigation, Formal analysis, Data curation, Conceptualization. **Hongsheng Wang:** Writing – review & editing, Writing – original draft, Investigation, Formal analysis, Conceptualization. **Yuntian Teng:** Writing – review & editing, Writing – original draft, Methodology, Investigation, Formal analysis. **Nino Ripepi:** Writing – review & editing, Writing – original draft, Resources, Project administration, Funding acquisition, Formal analysis. **Carlos A. Fernandez:** Writing – review & editing, Writing – original draft, Supervision, Resources, Investigation. **Cheng Chen:** Writing – review & editing, Writing – original draft, Validation, Supervision, Resources, Project administration, Methodology, Investigation, Funding acquisition, Formal analysis, Conceptualization.

Declaration of competing interest

There are no conflicts of interest associated with this work.

Acknowledgment

The authors acknowledge the funding support from the U.S. Department of Energy through the National Energy Technology Laboratory under Contract No. DE-FE0031576 and the technical support from Zygote Corporation. The authors also greatly appreciate the valuable feedback provided by Dr. Nicolas J. Huerta from the Pacific Northwest National Laboratory, which significantly contributed to the improvement of this paper.

Data availability

Data will be made available on request.

References

- Ahamed, M.A.A., Perera, M.S.A., Dong-yin, L., Ranjith, P.G., Matthai, S.K., 2019. Proppant damage mechanisms in coal seam reservoirs during the hydraulic fracturing process: a review. *Fuel* 253, 615–629.
- American Petroleum Institute, 2021. Measuring Conductivity of Proppants, second ed. API RP 19D.
- Belyadi, H., Fathi, E., Belyadi, F., 2017. Chapter Six-Proppant characteristics and application design. *Hydraulic Fracturing in Unconventional Reservoirs*. Gulf Professional Publishing, Boston, pp. 73–96.
- Bijay, K.C., Ghazanfari, E., 2021. Geothermal reservoir stimulation through hydro-shearing: an experimental study under conditions close to enhanced geothermal systems. *Geothermics* 96, 102200.
- Breede, K., Dzebisashvili, K., Liu, X., Falcone, G., 2013. A systematic review of enhanced (or engineered) geothermal systems: past, present and future. *Geoth. Energy* 1, 1–27.
- Chen, C., Lau, B.L., Gaillard, J.F., Packman, A.I., 2009. Temporal evolution of pore geometry, fluid flow, and solute transport resulting from colloid deposition. *Water Resour. Res.* 45 (6).

- Chen, C., Martysevich, V., O'Connell, P., Hu, D., Matzar, L., 2015. Temporal evolution of the geometrical and transport properties of a fracture/proppant system under increasing effective stress. *SPE J.* 20 (3), 527–535.
- Childers, I.M., Endres, M., Burns, C., Garcia, B.J., Liu, J., Wietsma, T.W., et al., 2017. Novel highly dispersible, thermally stable core/shell proppants for geothermal applications. *Geothermics* 70, 98–109.
- Cooke Jr, C.E., 1973. Conductivity of fracture proppants in multiple layers. *J. Petrol. Technol.* 25 (9), 1101–1107.
- Deng, J., Hill, A.D., Zhu, D., 2011. A theoretical study of acid-fracture conductivity under closure stress. *SPE Prod. Oper.* 26 (1), 9–17.
- Fan, M., McClure, J., Han, Y., Ripepi, N., Westman, E., Gu, M., Chen, C., 2019. Using an experiment/simulation-integrated approach to investigate fracture conductivity evolution and non-Darcy flow in a proppant-supported hydraulic fracture. *SPE J.* 24 (4), 1912–1928. SPE-195588-PA.
- Fan, M., Li, Z., Han, Y., Teng, Y., Chen, C., 2021. Experimental and numerical investigations of the role of proppant embedment on fracture conductivity in narrow fractures (includes associated errata). *SPE J.* 26 (1), 324–341.
- Fardin, N., Feng, Q., Stephansson, O., 2004. Application of a new in situ 3D laser scanner to study the scale effect on the rock joint surface roughness. *Int. J. Rock Mech. Min. Sci.* 41 (2), 329–335.
- Geng, M., Xianbo, S., Haixiao, L., Hongyu, G., Yunqi, T., Xiao, L., 2014. Theory and technique of permeability enhancement and coal mine gas extraction by fracture network stimulation of surrounding beds and coal beds. *Nat. Gas. Ind. B* 1 (2), 197–204.
- Ghassemi, A., 2012. A review of some rock mechanics issues in geothermal reservoir development. *Geotech. Geol. Eng.* 30, 647–664.
- Gong, Y., Mehana, M., El-Monier, I., Viswanathan, H., 2020. Proppant placement in complex fracture geometries: a computational fluid dynamics study. *J. Nat. Gas Sci. Eng.* 79, 103295.
- Guo, R., Dalton, L., Crandall, D., McClure, J., Wang, H., Li, Z., Chen, C., 2022. Role of heterogeneous surface wettability on dynamic immiscible displacement, capillary pressure, and relative permeability in a CO₂-water-rock system. *Adv. Water Resour.* 165, 104226.
- Guo, R., Dalton, L.E., Fan, M., McClure, J., Zeng, L., Crandall, D., Chen, C., 2020. The role of the spatial heterogeneity and correlation length of surface wettability on two-phase flow in a CO₂-water-rock system. *Adv. Water Resour.* 146, 103763.
- Han, J., Wang, J.Y., Puri, V., 2014. A fully coupled geomechanics and fluid flow model for proppant pack failure and fracture conductivity damage analysis. In: SPE Hydraulic Fracturing Technology Conference. OnePetro.
- Huang, J., Hao, Y., Settgast, R.R., White, J.A., Mateen, K., Gross, H., 2022. Validation and application of a three-dimensional model for simulating proppant transport and fracture conductivity. *Rock Mech. Rock Eng.* 1–23.
- Ju, Y., Zhang, Q., Zheng, J., Chang, C., Xie, H., 2017. Fractal model and lattice Boltzmann method for characterization of non-Darcy flow in rough fractures. *Sci. Rep.* 7 (1), 41380.
- Klinkenberg, L.J., 1941. The permeability of porous media to liquids and gases. In: Paper Presented at the Drilling and Production Practice. New York, New York, USA, 1 January. API-41-200.
- Lee, D.S., Herman, J.D., Elsworth, D., Kim, H.T., Lee, H.S., 2011. A critical evaluation of unconventional gas recovery from the marcellus shale, northeastern United States. *KSCE J. Civ. Eng.* 15, 679–687.
- Li, K., Gao, Y., Lyu, Y., Wang, M., 2015. New mathematical models for calculating proppant embedment and fracture conductivity. *SPE J.* 20 (3), 496–507.
- Li, Z., Ripepi, N., Chen, C., 2020. Using pressure pulse decay experiments and a novel multi-physics shale transport model to study the role of Klinkenberg effect and effective stress on the apparent permeability of shales. *J. Petrol. Sci. Eng.* 189, 107010.
- Li, Z., Teng, Y., Fan, M., Ripepi, N., Chen, C., 2022a. A novel multiphysics multiscale multiporosity shale gas transport model for geomechanics/flow coupling in steady and transient states. *SPE J.* 27 (1), 452–464.
- Li, Z., Zhao, Q., Teng, Y., Fan, M., Ripepi, N., Yin, X., Chen, C., 2022b. Experimental investigation of non-monotonic fracture conductivity evolution in energy georeservoirs. *J. Petrol. Sci. Eng.* 211, 110103.
- Liang, F., Sayed, M., Al-Muntasher, G.A., Chang, F.F., Li, L., 2016. A comprehensive review on proppant technologies. *Petroleum* 2 (1), 26–39.
- Luo, J., Zhang, Q., Elsworth, D., Zhao, Q., 2023. Competing effects of proppant and surface roughness on the frictional stability of propped fractures. *Rock Mech. Rock Eng.* 56 (4), 2923–2934.
- Nadimi, S., Forbes, B., Moore, J., Podgornay, R., McLennan, J.D., 2020. Utah FORGE: hydrogeothermal modeling of a granitic based discrete fracture network. *Geothermics* 87, 101853.
- Osiptsov, A.A., Garagash, I.A., Boronin, S.A., Tolmacheva, K.I., Lezhnev, K.E., Paderin, G. V., 2020. Impact of flowback dynamics on fracture conductivity. *J. Petrol. Sci. Eng.* 188, 106822.
- Phillips, T., Kampman, N., Bisdom, K., Inskip, N.D.F., den Hartog, S.A., Cnudde, V., Busch, A., 2020. Controls on the intrinsic flow properties of mudrock fractures: a review of their importance in subsurface storage. *Earth Sci. Rev.* 211, 103390.
- Qu, H., Xu, Y., Liu, Y., Li, Z., Liu, X., Zeng, Z., Guo, R., 2023a. Experimental study of fluid-particle flow characteristics in a rough fracture. *Energy* 285, 129380.
- Qu, H., Hong, J., Liu, Y., Zeng, Z., Liu, X., Chen, X., Guo, R., 2023b. Experiment and simulation of slurry flow in irregular channels to understand proppant transport in complex fractures. *Particulology* 83, 194–211.
- Rahm, D., 2011. Regulating hydraulic fracturing in shale gas plays: the case of Texas. *Energy Pol.* 39 (5), 2974–2981.
- Salvinini, R., Vanneschi, C., Coggan, J.S., Mastrorocco, G., 2020. Evaluation of the use of UAV photogrammetry for rock discontinuity roughness characterization. *Rock Mech. Rock Eng.* 53, 3699–3720.
- Schmidt, D., Rankin, P.R., Williams, B., Palisch, T., Kullman, J., 2014. Performance of mixed proppant sizes. In: SPE Hydraulic Fracturing Technology Conference and Exhibition, pp. SPE-168629. SPE.
- Simo, H., Pournik, M., Sondergeld, C.H., 2013. Proppant crush test: a new approach. In: SPE Oklahoma City Oil and Gas Symposium/Production and Operations Symposium, pp. SPE-164506. SPE.
- Sun, W., Kuhn, M.R., Rudnicki, J.W., 2013. A multiscale DEM-LBM analysis on permeability evolutions inside a dilatant shear band. *Acta Geotechnica* 8, 465–480.
- Tan, Y., Pan, Z., Liu, J., Feng, X.T., Connell, L.D., 2018. Laboratory study of proppant on shale fracture permeability and compressibility. *Fuel* 222, 83–97.
- Tonietto, L., Gonzaga Jr, L., Veronez, M.R., Kazmierczak, C.D.S., Arnold, D.C.M., Costa, C.A.D., 2019. New method for evaluating surface roughness parameters acquired by laser scanning. *Sci. Rep.* 9 (1), 15038.
- Tong, S., Mohanty, K.K., 2016. Proppant transport study in fractures with intersections. *Fuel* 181, 463–477.
- Vijayababu, T.R., Dhinakaran, S., 2019. MHD Natural convection around a permeable triangular cylinder inside a square enclosure filled with Al₂O₃–H₂O nanofluid: an LBM study. *Int. J. Mech. Sci.* 153, 500–516.
- Wang, H., Sharma, M.M., 2018. Estimating unpropped-fracture conductivity and fracture compliance from diagnostic fracture-injection tests. *SPE J.* 23 (5), 1648–1668.
- Wang, J., Elsworth, D., 2018. Role of proppant distribution on the evolution of hydraulic fracture conductivity. *J. Petrol. Sci. Eng.* 166, 249–262.
- Wang, T., Wang, P., Yin, Z.Y., Laouafa, F., Hicher, P.Y., 2024a. Hydro-mechanical analysis of particle migration in fractures with CFD-DEM. *Eng. Geol.* 335, 107557.
- Wang, Y.D., Chung, T., Armstrong, R.T., Mostaghimi, P., 2021. ML-LBM: predicting and accelerating steady state flow simulation in porous media with convolutional neural networks. *Transport Porous Media* 138 (1), 49–75.
- Wang, Z., Peng, C., Ayala, L.F., Hosseini, S., 2024b. A Framework for Simulating the Partially Miscible Multi-Component Hydrocarbon Fluids in Porous Media via the Pseudo-potential Lattice Boltzmann Model. Available at: SSRN 4576831.
- Warpinski, N.R., Mayerhofer, M.J., Vincent, M.C., Cipolla, C.L., Lolon, E.P., 2009. Stimulating unconventional reservoirs: maximizing network growth while optimizing fracture conductivity. *J. Can. Petrol. Technol.* 48 (10), 39–51.
- Yi, J., Xing, H., Wang, J., Xia, Z., Jing, Y., 2019. Pore-scale study of the effects of surface roughness on relative permeability of rock fractures using lattice Boltzmann method. *Chem. Eng. Sci.* 209, 115178.
- Yu, W., Zhang, T., Du, S., Sepehnoori, K., 2015. Numerical study of the effect of uneven proppant distribution between multiple fractures on shale gas well performance. *Fuel* 142, 189–198.
- Zhang, F., Damjanac, B., Maxwell, S., 2019. Investigating hydraulic fracturing complexity in naturally fractured rock masses using fully coupled multiscale numerical modeling. *Rock Mech. Rock Eng.* 52 (12), 5137–5160.
- Zhang, F., Zhu, H., Zhou, H., Guo, J., Huang, B., 2017. Discrete-element-method/computational-fluid-dynamics coupling simulation of proppant embedment and fracture conductivity after hydraulic fracturing. *SPE J.* 22 (2), 632–644.